Method for in-flight satellite calibration in the ultraviolet using radiative transfer calculations, with application to Scanning Imaging Absorption Spectrometer for Atmospheric Chartography (SCIAMACHY)

L. G. Tilstra, G. van Soest, and P. Stammes
Royal Netherlands Meteorological Institute, De Bilt, Netherlands

Received 8 February 2005; revised 11 May 2005; accepted 22 June 2005; published 29 September 2005.

[1] We present a reflectance validation method, using a polarized radiative transfer model as a reference. The method involves calculating the complete radiative transfer in the ultraviolet for a carefully selected, natural, cloud-free Earth target. An extensive sensitivity study shows that in the ultraviolet, the ozone profile (mainly below 330 nm) and the surface albedo (mainly above 330 nm) are the important parameters that affect the reflectance and are therefore the major sources of error in the modeled reflectances. The accuracy with which the reflectance in the UV range of 240–400 nm can be calculated, because of uncertainty in input parameters, is 2–6%, depending on wavelength. The method is applied to Scanning Imaging Absorption Spectrometer for Atmospheric Chartography (SCIAMACHY), using a cloud-free scene over the Sahara desert. The reflectance measured by SCIAMACHY turns out to show a scan-angle-independent calibration error of 10–25% for this particular Sahara target. The result is confirmed for ocean and vegetation targets.

Citation: Tilstra, L. G., G. van Soest, and P. Stammes (2005), Method for in-flight satellite calibration in the ultraviolet using radiative transfer calculations, with application to Scanning Imaging Absorption Spectrometer for Atmospheric Chartography (SCIAMACHY), *J. Geophys. Res.*, *110*, D18311, doi:10.1029/2005JD005853.

1. Introduction

[2] Satellite monitoring of atmospheric chemical composition started with the Total Ozone Mapping Spectrometer (TOMS) series of instruments (1979 to present), measuring the Earth reflectance at six UV wavelengths between about 310 and 380 nm. From these limited spectral measurements, global daily observations of ozone column, and other products like SO_2 and absorbing aerosols, have been determined, creating the longest climate data set from satellite. The range of spectral information has increased enormously with the introduction of the spectrometers Global Ozone Monitoring Experiment (GOME) (launched in 1995, covering the range 240–800 nm [*Burrows et al.*, 1999]) and Scanning Imaging Absorption Spectrometer for Atmospheric Chartography (SCIAMACHY) (launched in March 2002, 240–2380 nm [*Bovensmann et al.*, 1999]). These instruments cover the spectral range that comprises the ultraviolet, visible, and near-infrared with a spectral resolution of about 0.2–1.5 nm. Using this spectral coverage and resolution, not only ozone and SO_2 but also NO_2, BrO, H_2CO, H_2O, CO_2, CO, and CH_4 can be determined.

0148-0227/05/2005JD005853$09.00

[3] However, accurate retrieval of these gases is only possible if the instrument behavior is well understood. Satellite instruments degrade faster in the UV than at longer wavelengths due to harsh space conditions. Therefore in-flight calibration and calibration monitoring is especially important in the UV. For TOMS, specific methods have been developed for calibration monitoring based on radiance residues of natural targets and the spectral discrimination method [*McPeters et al.*, 1996, 1998; *Wellemeyer et al.*, 1996]. Knowledge of absolute radiometric calibration is less important for trace gas retrievals from GOME and SCIAMACHY than it is for TOMS, because of the differential optical absorption spectroscopy (DOAS) retrieval method. In the DOAS retrieval method [*Platt*, 1994], only differential absorption structures of trace gases are used, which is possible by the virtue of the many wavelengths observed. Any constant radiometric error cancels out in the DOAS method. At the same time, absolute calibration is essential for a number of other scientific products that are retrieved from the UV spectrum. Examples are the retrieval of the ozone profile [*Munro et al.*, 1998; *Hoogen et al.*, 1999; *Spurr*, 2001; *van der A et al.*, 2002; *Hasekamp et al.*, 2002; *Meijer et al.*, 2003], the absorbing aerosol index [*Herman et al.*, 1997; *Torres et al.*, 1998; *de Graaf et al.*, 2005], and surface albedo [*Herman and Celarier*, 1997; *Koelemeijer et al.*, 2003]. These types of retrievals rely on a correct absolute calibration of the UV radiances.

[4] GOME and SCIAMACHY are able to perform in-flight calibration measurements that can be used for monitoring of the instrument. Both measure the solar signal (irradiance) on a daily basis to be able to normalize the Earth signals (radiances) they collect. In addition, they measure polarization for every radiance measurement to correct for the instrument's sensitivity to atmospheric polarization. Changes in the radiometric response of these instruments, which are caused by degradation of the optics, are recorded by the daily measured solar signal. This allows performing a correction on the radiometric response that was determined preflight.

[5] However, the assumption made here is that the solar signal and the Earth signal are likely to degrade in the same manner. This is not always the case [see, e.g., *van der A et al.*, 2002], and in these cases the approach does not cure degradation of the ratio between the Earth radiance and solar irradiance, the so-called reflectance (especially noticeable in the UV).

[6] This paper introduces a method for validating the satellite measured reflectance in the ultraviolet wavelength range. We focus on a stable and cloud-free natural Earth target. For such a target, Rayleigh scattering, ozone absorption, surface reflection, aerosol presence and residual cloud contamination are the dominant factors contributing to the top-of-atmosphere (TOA) signal. We combine the measured radiance and irradiance signals into a reflectance on the one hand and try to model the reflectance with a radiative transfer model on the other hand. This Rayleigh type of comparison may also be helpful in the in-flight calibration of the new UV-visible spectrometers Ozone Monitoring Instrument (OMI) [*Levelt et al.*, 2002] (launched in July 2004) and GOME-2 [*Callies et al.*, 2000] (to be launched in 2006).

[7] We should mention that in-flight calibration using a model reflectance has been used before. Instruments like Polarization and Directionality of the Earth's Reflection (POLDER) [*Deschamps et al.*, 1994] and Medium-Resolution Imaging Spectrometer (MERIS) [*Rast et al.*, 1999; *Santer et al.*, 2005] use model calculations for fine tuning of their calibration [see, e.g., *Hagolle et al.* 1999].

[8] The outline of the paper is as follows. In section 2 we start with a short description of the SCIAMACHY instrument and the quantity of interest, which is the Earth reflectance. Section 3 introduces the principle of the calibration validation method presented in this paper, which is a comparison of the instrument's reflectance with that of a radiative transfer model in the UV. Section 4 presents a sensitivity study investigating the sensitivity of the model reflectance to the various input parameters, such as the ozone profile, surface albedo, surface pressure, and aerosol load. In section 5 we present the results of a reflectance calibration validation for the SCIAMACHY instrument. We apply the knowledge gained from the sensitivity study to these results. An error estimation is given and the applicability of the method is discussed. A conclusion is given in section 6.

2. SCIAMACHY and Its Calibration

[9] SCIAMACHY is a remote sensing spectrometer capable of performing Earth radiance measurements over the wavelength range between about 240 and 2400 nm, with a spectral resolution ranging from 0.24 nm in the UV to 1.56 nm in the near infrared. The instrument is situated onboard the Envisat satellite, which was launched on 1 March 2002. The Envisat platform was put into a polar Sun-synchronous orbit at an altitude of 800 km, with a local crossing time of the equator of 1000 LT for the descending node. One of the merits of SCIAMACHY is its ability to perform radiance measurements in either nadir or limb mode [*Bovensmann et al.*, 1999]. These modes usually alternate and a contiguous measurement series in either mode is called a "state." Owing to this pattern of nadir and limb measuring modes, the instrument is able to observe the same atmospheric volume first in limb and then about 7 min later in nadir viewing geometry.

[10] In this paper we will concentrate on the nadir mode of the instrument. The size of a typical nadir state is approximately 960×490 km^2 (across track $\times$ along track). This area is determined by the scan speed of the nadir mirror (in the across track direction), the spacecraft speed (in the along-track direction), the instrument field of view, and instrument operation. A full scan of the nadir mirror, which starts scanning from east to west, and then back, always lasts five seconds. As a consequence, the size of an individual pixel in nominal measurement mode can only be influenced by the scan speed of the nadir mirror and the integration time (IT) of the instrument. Typical pixel sizes are 60×30 km^2 (for an IT of 0.25 s) and 240×30 km^2 (for an IT of 1.0 s).

[11] The scientific goal of SCIAMACHY is to perform global measurements of various trace gases in the troposphere and stratosphere, which are retrieved from the Earth radiance spectra. These trace gases include ozone, NO_2, CH_4, CO, and a variety of other trace gases [*Bovensmann et al.*, 1999]. Apart from this, SCIAMACHY also monitors aerosol presence and retrieves cloud information. The atmospheric profiles for certain trace gases are being retrieved using the limb scanning mode of the instrument. All these level 2 products are currently being validated [*European Space Agency*, 2004].

[12] At the basis of these level 2 products lies the main level 1 product, namely, the Earth reflectance. In this paper we will therefore focus on the Earth reflectance R in nadir, defined as

$$R = \frac{\pi I}{\mu_0 E}, \tag{1}$$

where I is the radiance reflected by the Earth atmosphere (in W m^{-2} nm^{-1} sr^{-1}), E is the incident solar irradiance at the top of the atmosphere perpendicular to the solar beam (in W m^{-2} nm^{-1}), and μ_0 is the cosine of the solar zenith angle θ_0. A typical SCIAMACHY reflectance spectrum is shown in Figure 1. During each orbit, SCIAMACHY measures the radiance I, while the solar irradiance E is measured once per day. Both can be expressed in terms of the raw instrument signals S_{Earth} and S_{Sun} in the following way:

$$I = c_{\mathrm{rad}}\, c_{\mathrm{pol}}\, S_{\mathrm{Earth}}, \qquad E = c_{\mathrm{irrad}}\, S_{\mathrm{Sun}}, \tag{2}$$

where all quantities depend on wavelength. The calibration constant c_{pol} corrects for the instrument's sensitivity to

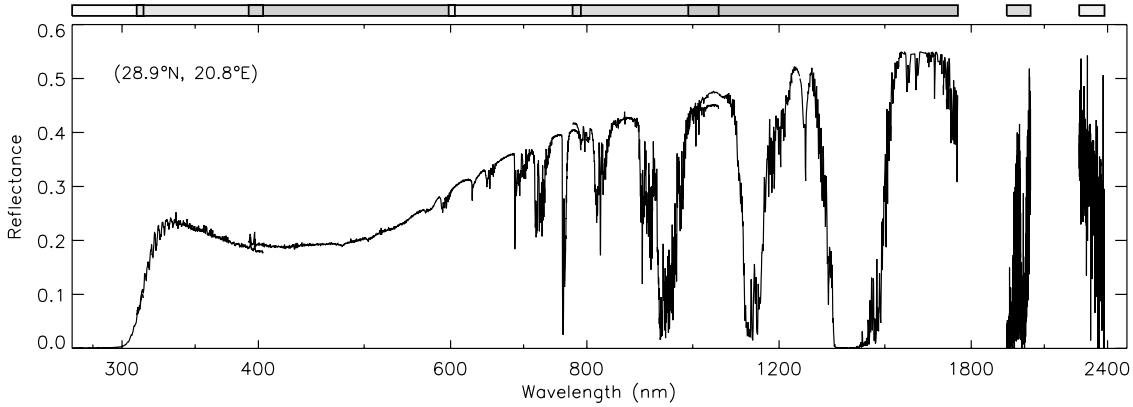

Figure 1. Example of a SCIAMACHY reflectance spectrum. The spectrum was taken over the Sahara desert. The bars on top of the graph illustrate the spectral ranges of the eight spectral channels, and their overlap, if any.

polarization and is scene-dependent, unlike c_{rad} and c_{irrad}, which are fixed (see section 5). The solar signal does not need to be corrected for polarization effects since sunlight is unpolarized.

3. Reflectance Validation Method

[13] We validate the Earth reflectance as measured by a satellite instrument by comparing with a reference spectrum. This method relies on a radiative transfer model (RTM) to provide the reference spectrum. The quantity we analyze is the relative difference between observed and simulated reflectance: $d_{\mathrm{R}} = (R_{\mathrm{obs}} - R_{\mathrm{sim}})/R_{\mathrm{sim}}$. The atmosphere and surface input parameters needed by the radiative transfer model are dictated by the specific scene observed by the spectrometer at hand (in this case, SCIAMACHY). Insufficient knowledge of the input parameters will turn out to be the main source of error in such a reflectance comparison. It is therefore best to minimize the amount of input parameters and the uncertainty they introduce. In practice, this means dealing with cloud-free scenes only. For the comparison presented in this paper, we selected a cloud-free scene over the Sahara desert.

3.1. Sahara Measurements

[14] Figure 2 gives an impression of the selected Sahara region and the measurements taken by the SCIAMACHY instrument. Indicated are two subsequent nadir states, which are both part of orbit 2509, taken on 23 August 2002 (software version 5.00). The lower state is the interesting one, since the observed Sahara region was completely free of clouds at the time of measurement. An additional advantage lies in the fact that no aerosols were present in the atmosphere that day, which was verified using Moderate Resolution Imaging Spectroradiometer (MODIS) [*King et al.*, 1992] aerosol data.

[15] Black lines delineate the pixels in this state of 0.25 s integration time (footprint size 60 × 30 km^2). SCIAMACHY's detectors are read out in blocks, called clusters, which can be configured to have different ITs. The integration time can therefore vary over the instrument's spectral range, depending on the signal strength and scientific interest. Other ITs that occur in nadir mode are 0.125 s, 0.5 s, and 1 s, where the ground pixel footprint becomes larger with larger IT. For the Sahara state under consideration, the largest cluster IT is 1 s, which means that in order to combine all of SCIAMACHY's clusters into a continuous spectrum describing the very same pixel, observations of ITs smaller than 1 s have to be binned together.

[16] This requirement inspired us to construct the four larger Sahara regions indicated in Figure 2. Their width is determined by four pixels of 0.25 s IT, and their height is determined by seven of these pixels such that the region is more or less square (240 × 210 km^2), sufficiently large, and located over a homogeneous surface. The four Sahara regions are labeled "east," "center-east," "center-west,"

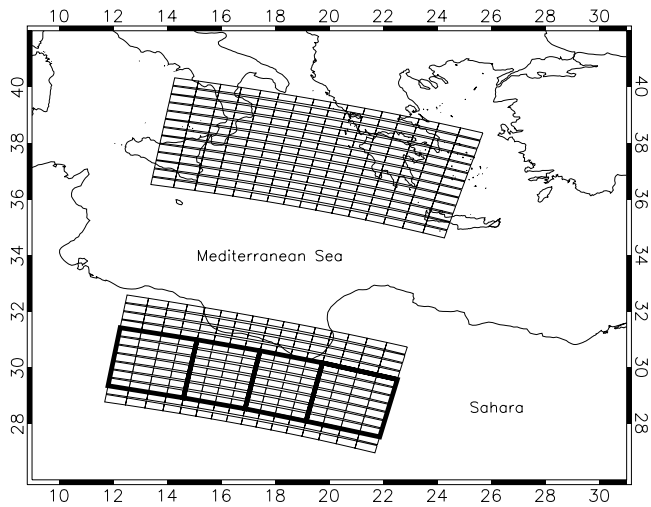

Figure 2. Explanation of the measurement approach followed by SCIAMACHY. Measurements are taken in blocks, called states, and nadir and limb states are both being measured in turns. The plot shows two subsequent nadir states; the lower one covers part of the Sahara desert. The smallest boxes indicate footprints of 0.25 s integration time (60 × 30 km^2). The four large regions in the lower state (size 240 × 210 km^2, delineated by thick lines) were constructed for the comparison presented in this paper.

Table 1. Scattering Geometries of the Four Sahara Regions[a]

Sahara Region	θ	θ_0	$\phi - \phi_0$	Θ
East	26.75°	27.52°	−20.22°	126.7°
Center-east	28.86°	29.27°	−18.96°	142.3°
Center-west	28.84°	30.87°	162.08°	157.4°
West	26.72°	32.64°	163.08°	169.8°

[a]Viewing zenith angle (θ), solar zenith angle (θ_0), and relative azimuth ($\phi - \phi_0$) are given. The single scattering angle Θ is given as well.

and "west." The scattering geometries associated with these regions are given in Table 1.

3.2. RTM Simulations

[17] To simulate the reflectances of the four Sahara regions, we made use of the polarized radiative transfer model Doubling-Adding KNMI (DAK) [*de Haan et al.*, 1987; *Stammes et al.*, 1989; *Stammes*, 2001]. This code is capable of calculating all four components of the Stokes vector at the top of the atmosphere. Because polarization is fully taken into account, errors caused by the usual neglect of polarization by radiative transfer models [*Mishchenko et al.*, 1994; *Stammes*, 1995] are absent. The only scattering process that is not included is Raman scattering. The accuracy of DAK is fully determined by the accuracy of the optical input parameters.

[18] The surface albedo for each of the aforementioned Sahara regions was determined using the GOME Lambert equivalent reflectivity (LER) database [*Koelemeijer et al.*, 2003]. We assumed Lambertian surface reflection; that is, we assume that the surface reflection is unpolarized. This is a good approximation for most surfaces [*Roger et al.*, 1994; *Nadal and Bréon*, 1999] and certainly for desert surfaces.

[19] The atmospheric profile was based on a standard "midlatitude summer" profile [*Anderson et al.*, 1986]; however, the shape of the ozone profile was determined from SCIAMACHY limb measurements (C. von Savigny, personal communication, 2004), while the ozone column value was available from GOME measurements and accessible at http://www.temis.nl/ [*van der A et al.*, 2000, 2002]. Clouds were not present at the time of SCIAMACHY's overpass, as was verified with MERIS [*Rast et al.*, 1999] and MODIS [*King et al.*, 1992] imagery. Aerosols were not included either. This completes the description of the scenarios used for the four Sahara regions indicated in Figure 2.

4. Reflectance Sensitivity Study

[20] We studied the sensitivity of the reflectance for cloud-free scenes such as the ones presented in section 3, to the following model input parameters: surface albedo, ozone column, ozone profile shape, surface pressure, and aerosol optical thickness. We first define the sensitivity of the reflectance to an atmospheric parameter x as

$$dR_\star/dx_\star = (dR/R)/(dx/x). \quad (3)$$

These derivatives were calculated from different runs made by the DAK radiative transfer code, by introduction of a small relative change dx/x in the parameter x and noting the effect dR upon the reflectance R. This approach, known as "finite differencing," was carried out for a variety of input parameters and atmospheric scenarios.

[21] Knowledge of these sensitivities is necessary to help assess the origins of systematic deviations found between observation and simulation of reflectance, and to demonstrate the accuracy and applicability of the reflectance validation method presented in this paper.

4.1. Atmospheric Scenarios

[22] The sensitivity study involved the calculation of a large number of atmospheric scenarios. The starting point of each was the scenario of the eastern Sahara region of 23 August 2002, which was then adapted with respect to the input parameter of interest. The specific scattering

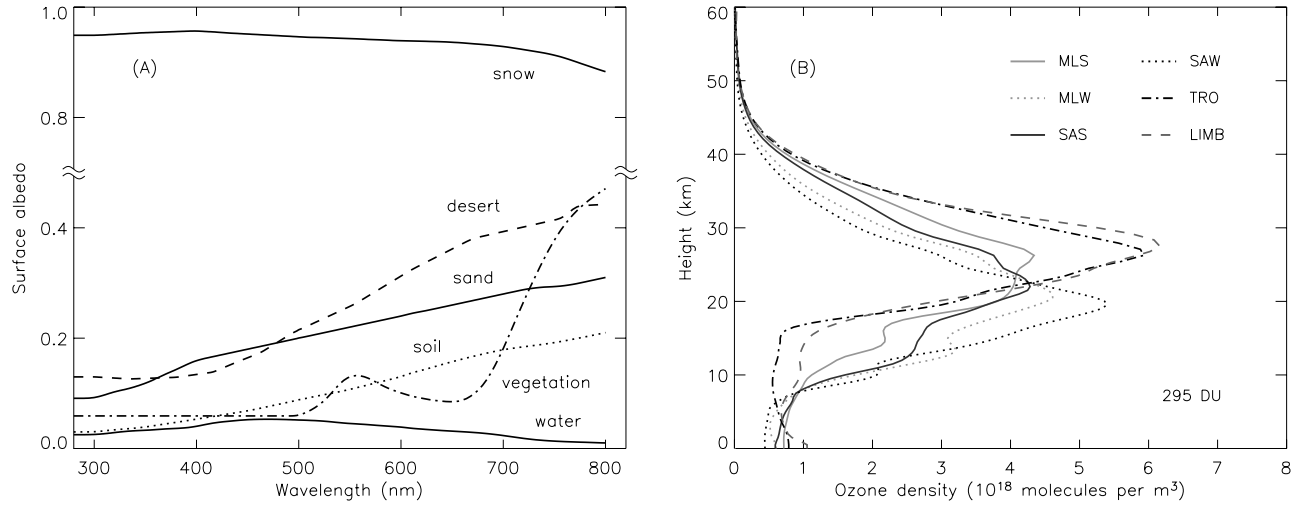

Figure 3. Input parameters used to build the various atmospheric scenarios used in the reflectance sensitivity study. (a) Standard surface albedos and the surface albedo of the eastern Sahara region (desert, dashed curve). (b) Set of climatological ozone profiles, plus the limb ozone profile. All ozone profiles were scaled to have an ozone column of 295 DU.

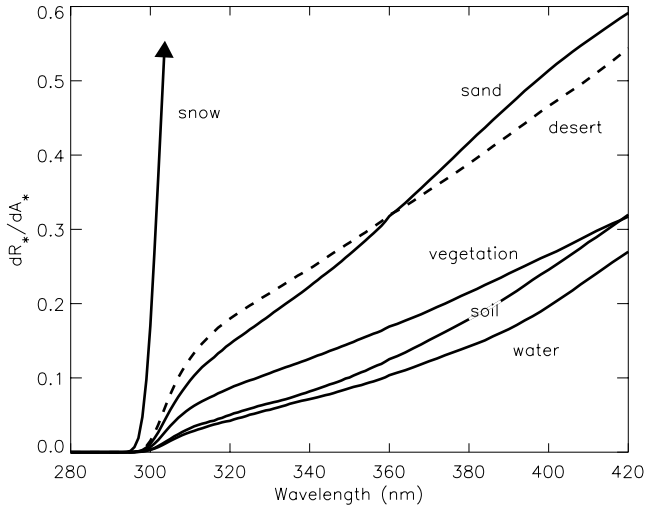

Figure 4. Sensitivity of the (TOA) reflectance to surface albedo in the UV as a function of wavelength for a cloud-free scene and calculated for a number of surface types. Desert refers to the surface albedo used for the Sahara site discussed in section 3.

geometry of this Sahara region can be found in Table 1. In Figure 3a the spectral surface albedo of the eastern Sahara region is plotted. This spectrum was taken from *Koelemeijer et al.* [2003]. The label used is "desert." In addition, standard surface albedo data for "snow," "water," "vegetation," "soil," and "sand" were also available [*Bowker et al.*, 1985]. These data are also shown in Figure 3a.

[23] The ozone profile, describing the vertical distribution of ozone for the eastern Sahara scene, followed from SCIAMACHY limb measurements (see section 3). Apart from using this limb ozone profile, we could rely on a set of climatological ozone profiles [*Anderson et al.*, 1986], including "midlatitude summer," "midlatitude winter," "subarctic summer," "subarctic winter," and "tropical." All these ozone profiles are shown in Figure 3b. For the sake of comparison, all profiles were scaled to 295 Dobson units (DU, 2.69×10^{16} molecules cm^{-2}), the ozone column of the Sahara region.

[24] Variations in surface pressure entailed only a change in the pressure field used for the radiative transfer calculations. Studying the influence of aerosols was realized by the addition of an aerosol layer with a Henyey-Greenstein phase function to the eastern Sahara scenario described above.

4.2. Sensitivity to Surface Albedo

[25] In Figure 4 we present the sensitivity of the reflectance to the surface albedo, defined as $dR_\star/dA_\star = (dR/R)/(dA/A)$, as a function of wavelength, for the eastern Sahara scenario, and for various surface types, including snow, water, vegetation, soil, and sand. The desert surface type, in Figure 4 presented by the dashed curve, is the original surface albedo belonging to the eastern Sahara region.

[26] Looking at Figure 4, it becomes clear that below a wavelength of, say, 300 nm, any possible error in the surface albedo will not influence the outcome of the comparison outlined in section 3. Above 300 nm, however, the surface albedo is having more and more impact on the reflectance because the atmosphere is becoming optically thinner with increasing wavelength. The exception to this behavior is displayed by the 'snow' surface type, for which at 300 nm the sensitivity rapidly increases up to 1.0, which is the asymptotic value reached by all the surface types at larger wavelengths if we neglect absorption.

[27] The implication of the result obtained here is that a typical accuracy like 10% in the surface albedo [see, e.g., *Koelemeijer et al.*, 2003] used for the model calculations can already introduce errors as high as 5% at a wavelength of 400 nm. For the Sahara region studied in this paper, we estimate the overall accuracy of the surface albedo to be about 10% as well. Generally speaking, such an accuracy allows a fair comparison for wavelengths up to 400 nm, but not much further than that. Finally, it was checked that for other geometries (i.e., other viewing angles) the plots are comparable to that of Figure 4.

4.3. Sensitivity to Ozone Profile

[28] In studying the sensitivity to the ozone profile, we first vary the ozone column while keeping the shape of the ozone profile constant. Next we vary the shape of the ozone profile, while keeping the ozone column constant.

[29] Figure 5 shows the sensitivity of the reflectance to the ozone column, $dR_\star/dO_{3\star} = (dR/R)/(dO_3/O_3)$, as a function of wavelength for three typical ozone values, and calculated for the eastern Sahara scenario described in section 3.2. The plot shows that above 330 nm the sensitivity to the ozone column is very small. Below 330 nm, the ozone column used has a large impact on the simulated reflectance, in particular in the region around 305 nm, where Rayleigh scattering and ozone absorption are the competing mechanisms for radiative transfer.

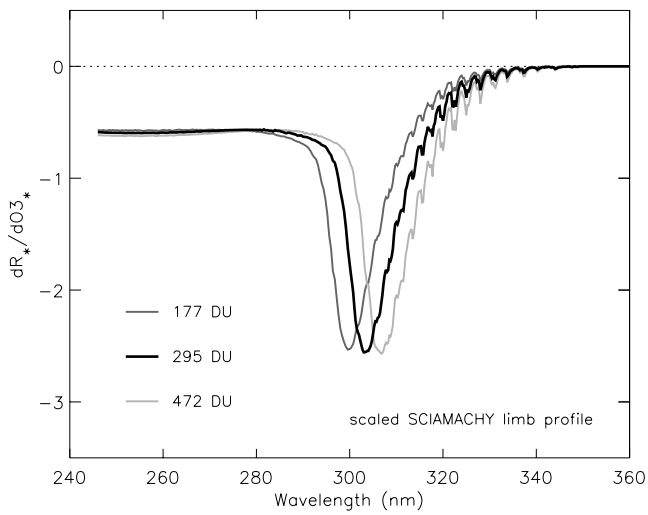

Figure 5. Sensitivity of the reflectance to the ozone column for three typical column values while the shape of the ozone profile was kept the same. Notice the sharp pit around 305 nm. It is the result of two competing processes: (multiple) Rayleigh scattering and ozone absorption. The position of the peak changes with the ozone column value used; its shape remains the same.

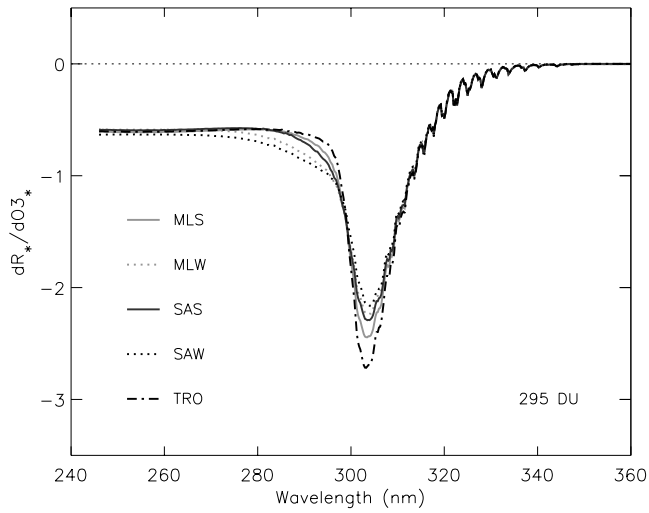

Figure 6. Sensitivity of the reflectance to the ozone profile, for five standard ozone profiles all scaled to an ozone column value of 295 DU. The position of the peak in the sensitivity does not change; the shape does.

[30] When the sensitivity is recalculated for alternative ozone column values, the resulting sensitivity curve keeps the same shape but changes its position in the spectrum. More specifically, it moves to the right when the calculations are done for higher ozone columns. The obvious next step is to change the shape of the ozone profile instead of the ozone column. The result of this exercise is presented in Figure 6, which shows the sensitivity for each of the five standard profiles presented in section 4.1. All ozone profiles were scaled to 295 DU. Now the position of the peak remains the same, but changes occur in the shape of the sensitivity curve.

[31] Therefore the specific shape of the assumed ozone profile will have an impact on the reflectance comparison discussed in this paper. To illustrate this, in Figure 7 we have plotted reflectance spectra assuming the five standard profiles relative to the reflectance assuming the SCIAMACHY limb ozone profile, for the eastern Sahara scenario. The specific ozone profile does not appear to be of any importance above 320 nm, but the effect it has on the shorter UV (below ~310 nm) is quite dramatic. The 'Midlatitude Summer' profile would have been the most logical candidate for the model atmospheric profile if the actual SCIAMACHY limb profile had not been available. Apparently, such a simplification would allow errors up to as much as 7% in the shorter UV.

[32] The relevance of Figures 5–7 for the model calculations to be presented in section 5 is that they predict a pronounced "spectral deviation" around 305 nm between simulation and measurement if a wrong ozone profile is used for the simulations. Such a feature, if it exists, will reveal any discrepancies in the ozone parameters used, and can therefore be used to fine tune these input parameters. In this way, a possible mismatch between simulation and measurement caused by an inaccurate ozone input parameter can be identified, and corrected, which can greatly improve the accuracy of the calibration validation technique presented in this paper. It was verified that calculations done for other geometries (e.g., other solar and viewing angles) result in plots quite similar to the ones shown in Figures 5–7.

4.4. Sensitivity to Surface Pressure

[33] Another parameter that may be important when performing model calculations of reflectances is the surface pressure p. In Figure 8 we plot the sensitivity $dR_\star/dp_\star = (dR/R)/(dp/p)$ as a function of wavelength, for a number of cases. Here dR/R is the relative change in the reflectance brought about by a change dp in the surface pressure p. The three solid curves represent the eastern Sahara scenario, equipped with the original desert surface albedo, or, alternatively, that of water or snow surfaces. The calculations were done for p = 1013 hPa, i.e., at sea level. For the desert and snow surfaces, we also calculated the sensitivity at a height of 5 km (p = 554 hPa). These results are given by the dotted curves.

[34] Below 300 nm, the sensitivity is zero, owing to the fact that at these wavelengths, light cannot effectively reach the lower part of the atmosphere because of strong ozone absorption [*Schutgens and Stammes*, 2002]. Even above 300 nm, the sensitivity does not reach serious proportions in view of the accuracy with which the surface pressure is generally known. Therefore surface pressure can be ruled out as a very important parameter for the present validation method.

4.5. Sensitivity to Aerosol Optical Thickness

[35] To study the sensitivity of the reflectance to the presence of Sahara dust aerosols, we introduced a layer of absorbing aerosols in the simulations. The aerosol layer consisted of Henyey-Greenstein scattering aerosols and was inserted between 1 and 2 km altitude. The Henyey-Greenstein phase function is defined as $\Phi(\Theta) = (1 - g^2)/(1 + g^2 - 2g\cos\Theta)^{3/2}$, where Θ is the scattering angle, and g the so-called asymmetry parameter [*Henyey and Greenstein*, 1941]. We chose g = 0.7 and the aerosol single scattering

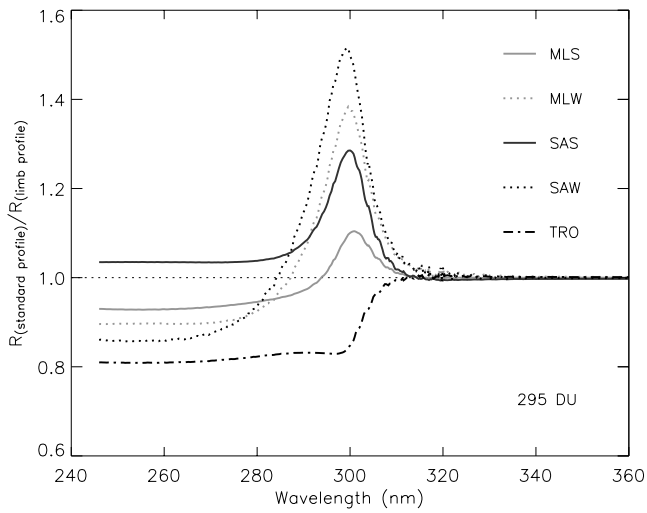

Figure 7. Reflectance calculated using the standard ozone profiles (scaled to 295 DU) divided by the reflectance obtained using the SCIAMACHY limb profile.

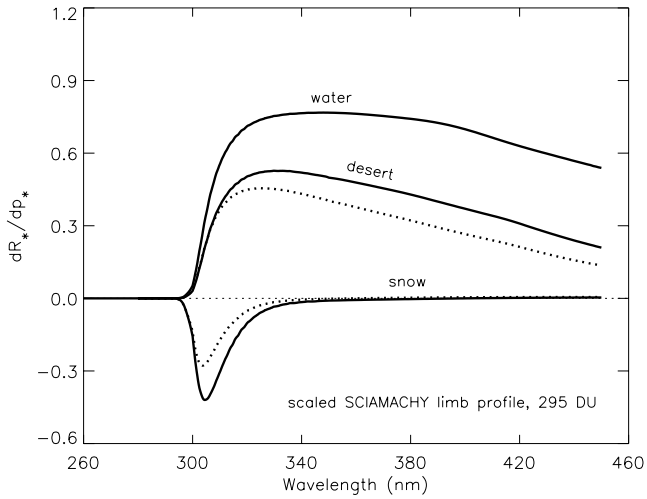

Figure 8. Sensitivity of the reflectance to surface pressure, computed at sea level for water, desert, and snow surface types (solid curves). For the desert and snow surfaces the sensitivities are given with respect to a height of 5 km as well (dotted curves).

albedo ω_0 was set to 0.8, representative of absorbing Sahara dust aerosol [*de Graaf et al.*, 2005]. The aerosol optical thickness τ_a was varied from 0.05 to 5. Figure 9 presents the sensitivity of the reflectance to the aerosol optical thickness, $dR_\star/d\tau_{a\star} = (dR/R)/(d\tau_a/\tau_a)$, as a function of wavelength for the eastern Sahara scenario.

[36] Below 300 nm, the sensitivity is zero, as expected. Above 300 nm, the sensitivity is growing with wavelength, and with increasing τ_a up to around $\tau_a = 1$. However, increasing the aerosol optical thickness even further lowers the sensitivity, owing to the fact that there is almost complete absorption by the aerosol layer at that point (instead of aerosol scattering and surface reflection which both increase the TOA signal).

[37] As for the importance of aerosols for the reflectance comparison presented in this paper, a simple estimate will show that aerosols have but a modest influence on the outcome. According to measurements, the Sahara region we focused on in this paper did not contain any dust aerosol load at the time of overpass of the SCIAMACHY instrument. Now suppose that this information was wrong and that the actual aerosol optical thickness was 1, not zero. Then according to Figure 9 we would have made an error $\Delta R/R$ less than $(\sim dR_\star/d\tau_{a\star})(\Delta\tau_a/\tau_a) = 0.04 \times 100\% = 4\%$ at 400 nm. Therefore, even a total neglect of aerosol presence in a worst-case scenario does not lead to excessive errors in the reflectance comparison.

4.6. Summary and Conclusion

[38] The sensitivity study clearly showed that the UV basically consists of two parts. Above about 330 nm, the exact shape of the ozone profile, as well as the actual ozone column value, have no significant impact on the reflectance. The only relevant parameters remaining thus are surface albedo, surface pressure and aerosol optical thickness. Of these, the surface albedo is the most important. Furthermore, the surface albedo is usually not known with a high accuracy, which limits the accuracy of a reflectance comparison especially at wavelengths above 400 nm.

[39] Below 330 nm, the situation is different. Surface albedo is unimportant (we only consider the case of cloud-free and ice/snow free scenes) but ozone column and profile both have a strong effect on the reflectance. Especially around 305 nm the effects are large, as is shown by, for example, Figure 5. Any discrepancy in the ozone profile will immediately result in a clear spectral feature in this area. This knowledge may in fact be used to fine tune the ozone profile.

5. Reflectance Comparison

[40] Before discussing the results of the reflectance comparison, we first have to address a problem with (current) SCIAMACHY reflectance data. The correction for the instrument's sensitivity to polarization is, at the time of writing, not performed at a satisfactory level. The resulting reflectance sometimes contains polarization features, that are either not removed by the polarization correction algorithm (PCA), or are falsely introduced by the PCA. This makes it hard to separate the quality of the radiometric calibration (c_{rad} and c_{irrad} in equation (2)) from the quality of the polarization correction (c_{pol} in equation (2)). This is in fact quite a general statement, valid not only for SCIAMACHY, but also for other spectrometers, like GOME and GOME-2.

[41] However, there is an elegant and reliable way out of this. The DAK radiative transfer model not only calculates the reflectance, but also the state of polarization of the radiation. It is therefore possible to perform a polarization correction on the instrument data ourselves. Details of this correction are given in section 5.1. After having discussed

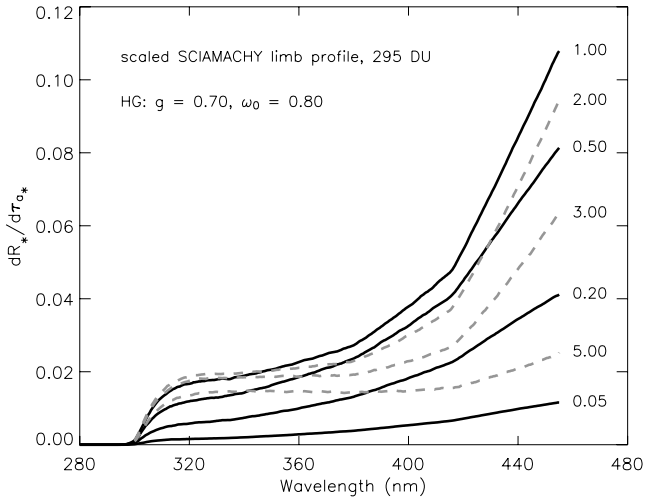

Figure 9. Sensitivity of the reflectance to aerosol optical thickness τ_a. The aerosol was assumed to scatter according to a Henyey-Greenstein phase function with $g = 0.7$ and to have a single-scattering albedo of 0.8. The sensitivity increases with increasing optical thickness up to $\tau_a = 1$, after which it starts to decrease with increasing optical thickness. Different line styles and colors help discriminate between both regimes, $\tau_a < 1$ and $\tau_a > 1$.

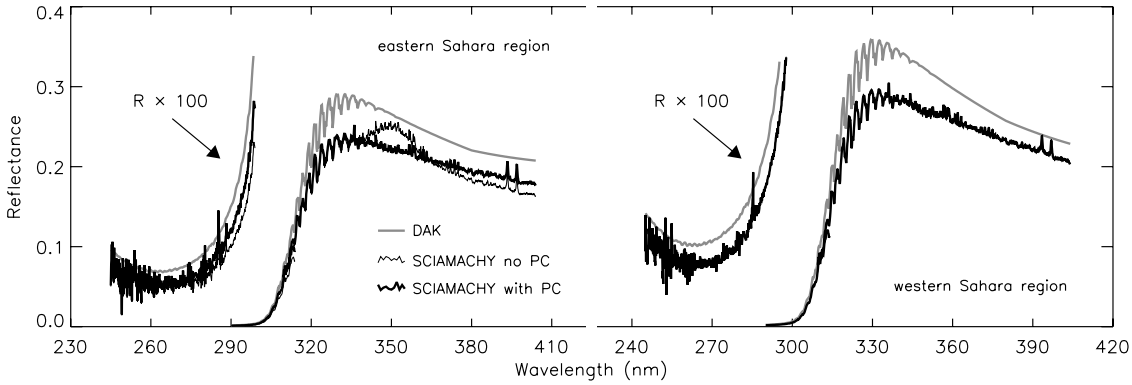

Figure 10. Reflectance as a function of wavelength, measured by SCIAMACHY and calculated using the radiative transfer code DAK. Reflectances are given for both the "eastern" and "western" Sahara regions discussed in section 3. Notice the different scaling used for the shorter UV. A polarization correction (PC) on the SCIAMACHY data could be applied using the polarization Stokes parameters provided by the DAK code.

the subject of polarization we will present the results of the reflectance calibration validation in section 5.2.

5.1. Polarization Correction

[42] Atmospheric radiation is usually described in terms of a four-component Stokes vector $\{I, Q, U, V\}$, in which the component I refers to the intensity of the radiation, and Q and U both characterize the degree and direction of linear polarization [*van de Hulst*, 1981]. The Stokes parameter V, denoting the degree of circular polarization, is very small, if not negligible, for most cases of atmospheric radiation [*Coulson*, 1988].

[43] The spectral channels of spectrometers like SCIAMACHY are generally sensitive to the polarization of the light that is being detected; the signal therefore not only depends on the amount of incident radiation, but also on the Stokes parameters Q and U describing the (linear) polarization of the light. More specifically, the instrument signal is being given by [*Slijkhuis*, 2001]

$$S_{\text{Earth}} = c_{\text{rad}}^{-1} I \left\{1 + \mu_2^D Q/I + \mu_3^D U/I\right\}, \tag{4}$$

where c_{rad}, μ_2^D, and μ_3^D are spectrally dependent calibration constants that are determined preflight. To obtain the radiance I from S_{Earth}, equation (4) should be inverted and this requires knowledge of the Stokes parameters Q and U. SCIAMACHY therefore measures polarization in-flight at a few wavelengths (six in total), using broadband polarization detectors, so-called PMDs.

[44] However, currently, the quality of the polarization parameters Q/I and U/I determined by SCIAMACHY is not up to the level required [*Tilstra and Stammes*, 2005], which is why in this paper the SCIAMACHY reflectance is corrected for polarization based on the Q/I and U/I obtained from simulations. In other words, the operational SCIAMACHY polarization correction is bypassed using our own polarization correction.

[45] It should be noted at this point that below ~300 nm, i.e., for SCIAMACHY's spectral channel 1, the polarization need not be measured but can be calculated from single scattering theory [*Schutgens and Stammes*, 2002, 2003; *Tilstra et al.*, 2003], as is done in the SCIAMACHY data processor [*Slijkhuis*, 2001]. As a result, our own polarization correction and that of the SCIAMACHY product are in full agreement below 300 nm.

5.2. First Results of the Comparison

[46] Figure 10 presents the UV part of the Earth's reflectance spectrum as a function of wavelength, for the eastern and western Sahara scenarios, measured by SCIAMACHY and calculated using DAK. The SCIAMACHY data is available with and without polarization correction (see section 5.1). Notice the difference between the SCIAMACHY reflectance of the eastern and western Sahara regions. The radiance of the eastern Sahara region, and hence the reflectance, shows a typical polarization feature around 350 nm if we do not correct for the instrument's sensitivity to polarization. For the western Sahara region, the Earth radiance is almost completely unpolarized owing to the near-backscattering viewing geometry (see Table 1), and therefore polarization features are absent. Figure 10 clearly shows how all polarization features are successfully removed by the scheme introduced in section 5.1.

[47] The main conclusion of Figure 10 is that the reflectance reported by SCIAMACHY is too low. Figure 11 shows by just how much. Here the relative difference d_{R} between SCIAMACHY and the DAK simulated reflectance is plotted between 240 and 400 nm, for spectral channels 1 and 2, and for all four Sahara regions indicated in Figure 2. The difference appears to be wavelength dependent, and ranges from −10% to as much as −30%. A clear viewing angle dependency is not found. Notice the "bump" around 305 nm. Acknowledging the results of section 4.3, it is most likely the result of a wrong shape picked for the ozone profile.

5.3. Recalculation and Error Analysis

[48] The sensitivity study has shown that the bump at 305 nm in Figure 11 is probably related to input errors in the ozone column or the shape of the ozone profile, or both. Given the fact that a complete removal of the bump, which

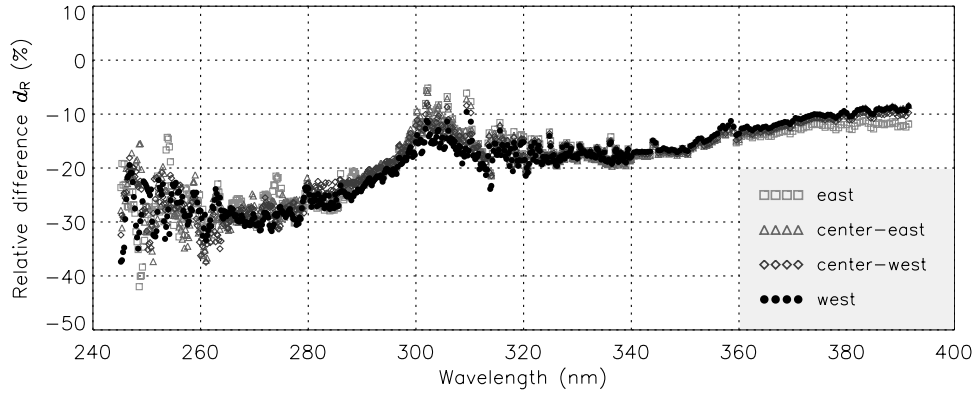

Figure 11. Relative difference between the reflectance measured by SCIAMACHY and the model calculations, presented as a function of wavelength for the four Sahara regions defined in section 3. The difference depends strongly on wavelength. The existence of a clear viewing geometry dependence can be excluded.

amounts to about 10% in Figure 11, would require an unrealistically high correction of 4% in the ozone column, we conclude that it is primarily the ozone profile shape that is at fault here.

[49] Indeed, the shape of the limb ozone profile that we used was retrieved from SCIAMACHY's own limb measurements (C. von Savigny, personal communication, 2004) and had not been perfected nor validated at the time of writing. This profile suffers from the Envisat pointing error, which was only corrected after December 2003. The consequences for the reflectance comparison presented in this paper were the following. We recalculated the simulated reflectance using the Midlatitude Summer (MLS) profile, and averaged the result over all four viewing angles. In exactly the same manner as before we calculated the difference between the reflectance measured by SCIAMACHY and that of the radiative transfer calculations. The result is presented in the top curve of Figure 12. As expected, the bump in the reflectance at 305 nm has decreased, indicating that the ozone input parameters were better chosen this time.

[50] From Figure 12 we now find that the bump is less than 2% in magnitude. This 2% error can easily be caused by a 1% error in the ozone column value (see Figure 5), which is even less than the reported accuracy of the ozone values we used. As we are more interested in presenting the type of method we used and the associated sensitivity study, rather than an extremely accurate value for the calibration error in the SCIAMACHY reflectance, we stop improving the accuracy of the comparison at this point.

[51] Figure 12 also shows similar results obtained for two completely different Earth scenes. The targets were a cloud-free part of the ocean (orbit 11251, software version 5.04; 17°S, 108°E) and a cloud-free scene over vegetated land (orbit 13028, software version 5.04; 51°N, 75°E). Both scenes have a minimal aerosol load. Standard atmospheric profiles were used, and the input parameters provided to the RTM were obtained from the same sources as before. The new results are in good agreement with the earlier result.

[52] Also given in Figure 12 are two "error curves" for the result of each Earth target. The accuracies they represent were based on the sensitivities found in the sensitivity study of section 4, combined with estimated accuracies for the input parameters. For the surface albedo, we estimated the error in the surface albedo to be about 10% for the "Sahara" scene, 20% for the "ocean" scene, and 15% for the "vegetation" scene [*Koelemeijer et al.*, 2003]. For the GOME ozone column we assumed an error of 2% [*Valks et al.*, 2003], and for the error in the profile we considered the ratio between reflectance of the midlatitude summer profile and the limb profile to be representative (see Figure 7). Surface pressure and aerosol presence are known with a high accuracy, and have low sensitivities, which is why they were not included in the analysis. The resulting total accuracy in the reflectance is ±2–4% at most wavelengths but about 6% around 305 nm.

6. Conclusion

[53] Performing an accurate in-flight reflectance validation in the UV using the reflectance of a polarized radiative transfer model as a reference requires a cloud-free scene for which an accurate ozone profile measured by, for example, an ozone sonde or a lidar, is available. Combined with modest knowledge of the surface albedo in the UV it is then possible to arrive at a meaningful, accurate comparison between measurement and model calculations between about 240 and 400 nm.

[54] This is shown by the reflectance sensitivity study. The main conclusion is that the UV can basically be divided into two areas: below 330 nm the ozone profile is the main parameter that determines the reflectance; above 330 nm, it is the surface albedo that is the dominant parameter. The degree of knowledge of these two parameters determines the accuracy of the model reflectance. The most striking consequence of improper input parameters is the occurrence of a bump in the deviation found between simulation and measurement around 305 nm when an inaccurate ozone profile is used for the model calculations. We showed that this feature can be used to fine tune the ozone profile in order to increase the accuracy of the reflectance comparison. Notice in this

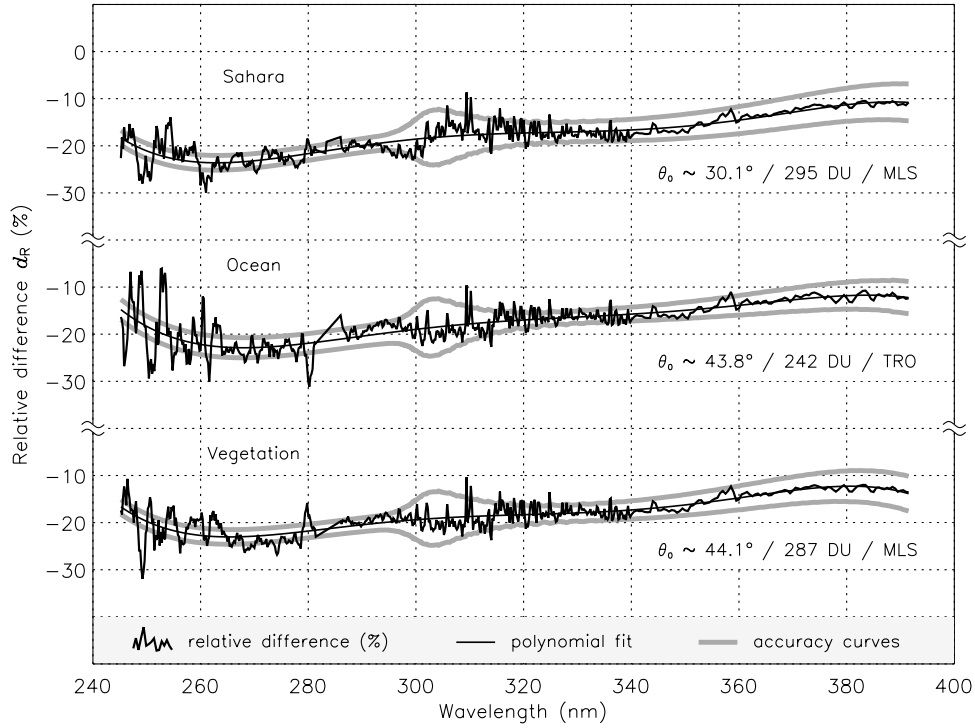

Figure 12. Relative difference between the reflectance measured by SCIAMACHY and that of the model calculations for the Sahara target (see Figure 11) and for two other Earth targets. Sahara target: Here we used a standard midlatitude summer ozone profile scaled to 295 DU instead of the ozone profile determined by limb measurements which was used in Figure 11. Since no clear viewing angle dependence was found, the data for different viewing angles were combined. A simple polynomial fit serves as a guide to the eye. Also indicated are error curves, based on the sensitivity study of section 4.

respect that the ozone column value is but only one characteristic property of the ozone profile.

[55] In this paper we focused on the reflectance of one satellite spectrometer, namely, SCIAMACHY. However, the type of comparison presented here may in fact be helpful in the in-flight calibration of other UV satellite spectrometers, like OMI and GOME-2. For satellite spectrometers like SCIAMACHY and GOME, an in-flight polarization correction is part of the radiometric calibration. In order not to be dependent on the quality of the operational polarization correction, we employed our own polarization correction, based on the polarization quantities provided by the (polarized) radiative transfer model. This correction works well.

[56] As for the validation of the reflectance measured by SCIAMACHY, we found a wavelength-dependent but scan-angle-independent discrepancy between measurement and model calculation for a number of independent Earth targets. The deviations range from −22% at 260 nm to −11% at 390 nm. It should be pointed out that these deviations are completely in line with the radiometric errors currently found for the visible wavelength range [*Noël*, 2004; *Gurlit et al.*, 2004; *Acarreta and Stammes*, 2005]. The reflectance correction factor c_R for SCIAMACHY in the UV can be constructed from Figure 12 using $c_R = 1/(1 + d_R)$.

[57] The strength of this new method is demonstrated by a first application of the method in the form of a large-scale, global validation of SCIAMACHY reflectances in the UV [*van Soest et al.*, 2005].

[58] **Acknowledgments.** The work presented in this publication was financed by the Netherlands Agency for Aerospace Programmes (NIVR). We would like to thank Christian von Savigny of IFE/IUP at the University of Bremen for supplying us with SCIAMACHY limb ozone profiles. The European Space Agency (ESA) and the Deutsches Zentrum für Luft- und Raumfahrt (DLR) are acknowledged for providing the SCIAMACHY data.

References

Acarreta, J. R., and P. Stammes (2005), Calibration comparison between SCIAMACHY and MERIS onboard ENVISAT, *IEEE Geosci. Remote Sens. Lett.*, *2*(1), 31–35, doi:10.1109/LGRS.2004.838348.

Anderson, G. P., S. A. Clough, F. X. Kneizys, J. H. Chetwynd, and E. P. Shettle (1986), AFGL atmospheric constituent profiles (0–120 km), *Environ. Res. Pap. 954, Rep. AFGL-TR-86-0110*, Air Force Geophys. Lab., Hanscom AFB, Mass.

Bovensmann, H., J. P. Burrows, M. Buchwitz, J. Frerick, S. Noël, V. V. Rozanov, K. V. Chance, and A. P. H. Goede (1999), SCIAMACHY: Mission objectives and measurement modes, *J. Atmos. Sci.*, *56*, 127–150.

Bowker, D. E., R. E. Davis, D. L. Myrick, K. Stacy, and W. T. Jones (1985), Spectral reflectances of natural targets for use in remote sensing studies, *NASA Ref. Publ., 1139*, 192 pp.

Burrows, J. P., et al. (1999), The Global Ozone Monitoring Experiment (GOME): Mission concept and first scientific results, *J. Atmos. Sci.*, *56*, 151–175.

Callies, J., E. Corpacciolli, M. Eisinger, A. Hahne, and A. Lefebvre (2000), GOME-2—Metop's second-generation sensor for operational ozone-monitoring, *ESA Bull.*, *102*, 28–36.

Coulson, K. L. (1988), *Polarization and Intensity of Light in the Atmosphere*, A. Deepak, Hampton, Va.

de Graaf, M., P. Stammes, O. Torres, and R. B. A. Koelemeijer (2005), Absorbing Aerosol Index: Sensitivity analysis, application to GOME and comparison with TOMS, *J. Geophys. Res.*, *110*, D01201, doi:10.1029/2004JD005178.

de Haan, J. F., P. B. Bosma, and J. W. Hovenier (1987), The adding method for multiple scattering calculations of polarised light, *Astron. Astrophys.*, *183*, 371–391.

Deschamps, P.-Y., F.-M. Bréon, M. Leroy, A. Podaire, A. Brickaud, J.-C. Buriez, and G. Sèze (1994), The POLDER mission: Instrument characteristics and scientific objectives, *IEEE Trans. Geosci. Remote Sens.*, *32*, 598–615.

European Space Agency (2004), Proceedings of the Second Workshop on the Atmospheric Chemistry Validation of ENVISAT (ACVE-2), *Spec. Publ. SP-562*, Paris.

Gurlit, W., et al. (2004), The UV-A and visible solar irradiance spectrum: Inter-comparison of absolutely calibrated, spectrally medium resolution solar irradiance spectra from balloon- and satellite-borne measurements, *Atmos. Chem. Phys. Discuss.*, *4*, 8439–8469.

Hagolle, O., P. Gouloub, P.-Y. Deschamps, H. Cosnefroy, X. Briottet, T. Bailleul, J.-M. Nicolas, F. Parol, B. Lafrance, and M. Herman (1999), Results of POLDER in-flight calibration, *IEEE Trans. Geosci. Remote Sens.*, *37*, 1550–1566.

Hasekamp, O. P., J. Landgraf, and R. van Oss (2002), The need of polarization modeling for ozone profile retrieval from backscattered sunlight, *J. Geophys. Res.*, *107*(D23), 4692, doi:10.1029/2002JD002387.

Henyey, L. G., and J. L. Greenstein (1941), Diffuse radiation in the galaxy, *Astrophys. J.*, *93*, 70–83.

Herman, J. R., and E. A. Celarier (1997), Earth surface reflectivity climatology at 340–380 nm from TOMS data, *J. Geophys. Res.*, *102*(D23), 28,003–28,011.

Herman, J. R., P. K. Bhartia, O. Torres, C. Hsu, C. Seftor, and E. Celarier (1997), Global distributions of UV-absorbing aerosols from Nimbus 7/TOMS data, *J. Geophys. Res.*, *102*(D14), 16,911–16,922, doi:10.1029/96JD03680.

Hoogen, R., V. V. Rozanov, and J. P. Burrows (1999), Ozone profiles from GOME satellite data: Algorithm description and first validation, *J. Geophys. Res.*, *104*(D7), 8263–8280.

King, M. D., Y. J. Kaufman, W. P. Menzel, and D. Tanré (1992), Remote sensing of cloud, aerosol, and water vapor properties from the Moderate Resolution Imaging Spectrometer (MODIS), *IEEE Trans. Geosci. Remote Sens.*, *30*, 2–27.

Koelemeijer, R. B. A., J. F. de Haan, and P. Stammes (2003), A database of spectral surface reflectivity in the range 335–772 nm derived from 5.5 years of GOME observations, *J. Geophys. Res.*, *108*(D2), 4070, doi:10.1029/2002JD002429.

Levelt, P. F., J. P. Veefkind, R. H. M. Voors, and J. de Vries (2002), OMI algorithm theoretical basis document: OMI instrument, level 0–1b processor, calibration and operations, *ATBD-OMI-01*, vol. I, NASA Goddard Space Flight Cent., Greenbelt, Md., Aug. (Available at http://eospso.gsfc.nasa.gov/eos_homepage/for_scientists/atbd/docs/OMI/ATBD-OMI-01.pdf)

McPeters, R. D., et al. (1996), Nimbus-7 Total Ozone Mapping Spectrometer (TOMS) data products users's guide, *NASA Ref. Publ., 1384*, 73 pp.

McPeters, R. D., et al. (1998), Earth probe Total Ozone Mapping Spectrometer (TOMS) data products user's guide, *NASA Tech. Publ. 1998-206895*, 70 pp.

Meijer, Y. J., R. J. van der A, R. F. van Oss, D. P. J. Swart, H. M. Kelder, and P. V. Johnston (2003), Global Ozone Monitoring Experiment ozone profile characterization using interpretation tools and lidar measurements for intercomparison, *J. Geophys. Res.*, *108*(D23), 4723, doi:10.1029/2003JD003498.

Mishchenko, M. I., A. A. Lacis, and L. D. Travis (1994), Errors induced by the neglect of polarization in radiance calculations for Rayleigh-scattering atmospheres, *J. Quant. Spectrosc. Radiat. Transfer*, *51*, 491–510.

Munro, R., R. Siddans, W. J. Reburn, and B. J. Kerridge (1998), Direct measurements of tropospheric ozone distributions from space, *Nature*, *392*, 168–171.

Nadal, F., and F.-M. Bréon (1999), Parametrization of surface polarized reflectance derived from POLDER spaceborne measurements, *IEEE Trans. Geosci. Remote Sens.*, *37*, 1709–1718.

Noël, S. (2004), Determination of correction factors for SCIAMACHY radiances and irradiances, *Tech. Note IFE-SCIA-SN-20040514*, Univ. of Bremen, Bremen, Germany.

Platt, U. (1994), Differential Optical Absorption Spectroscopy (DOAS), in *Air Monitoring by Spectroscopic Techniques*, Chemical Analysis Series, vol. 127, edited by M. W. Sigrist, pp. 27–84, John Wiley, Hoboken, N. J.

Rast, M., J. L. Bezy, and S. Bruzzi (1999), The ESA Medium Resolution Imaging Spectrometer MERIS—A review of the instrument and its mission, *Int. J. Remote Sens.*, *20*, 1681–1702.

Roger, J. C., R. Santer, M. Herman, and J. L. Deuzé (1994), Polarization of the solar light scattered by the Earth-atmosphere system as observed from the U.S. shuttle, *Remote Sens. Environ.*, *48*, 275–290.

Santer, R., N. Martiny, and I. Smolskaia (2005), Vicarious calibration of MERIS over dark waters in the near infrared, *Eur. Space Agency Spec. Publ., SP-572*.

Schutgens, N. A. J., and P. Stammes (2002), Parametrisation of Earth's polarisation spectrum in the ultra-violet, *J. Quant. Spectrosc. Radiat.*, *75*, 239–255.

Schutgens, N. A. J., and P. Stammes (2003), A novel approach to the polarization correction of spaceborne spectrometers, *J. Geophys. Res.*, *108*(D7), 4229, doi:10.1029/2002JD002736.

Slijkhuis, S. (2001), SCIAMACHY level 0 to 1c processing algorithm theoretical basis document, *Tech. Note ENV-ATB-DLR-SCIA-0041*, Dtsch. Zent. für Luft- und Raumfahrt, Oberpfaffenhofen, Germany.

Spurr, R. J. D. (2001), Linearized radiative transfer theory: A general discrete ordinate approach to the calculation of radiances and analytic weighting functions, with application to atmospheric remote sensing, Ph.D. thesis, Tech. Univ. Eindhoven, Eindhoven, Netherlands.

Stammes, P. (1995), Errors in UV reflectivity and albedo calculations due to neglecting polarization, in *Atmospheric Sensing and Modelling*, vol. 2311, edited by R. P. Santer, pp. 227–235, SPIE, Rome, Italy.

Stammes, P. (2001), Spectral radiance modelling in the UV-visible range, in *IRS 2000: Current Problems in Atmospheric Radiation*, edited by W. L. Smith and Y. M. Timofeyev, pp. 385–388, A. Deepak, Hampton, Va.

Stammes, P., J. F. de Haan, and J. W. Hovenier (1989), The polarized internal radiation field of a planetary atmosphere, *Astron. Astrophys.*, *225*, 239–259.

Tanzi, C. P., R. Snel, and I. Aben (2001), Degradation of observations in the UV of the Global Ozone Monitoring Experiment (GOME), in *IRS 2000: Current Problems in Atmospheric Radiation*, edited by W. L. Smith and Y. M. Timofeyev, pp. 181–184, A. Deepak, Hampton, Va.

Tilstra, L. G., and P. Stammes (2005), Alternative polarisation retrieval for SCIAMACHY in the ultraviolet, *Atmos. Chem. Phys. Discuss.*, *5*, 1973–1993.

Tilstra, L. G., N. A. J. Schutgens, and P. Stammes (2003), Analytical calculation of Stokes parameters Q and U of atmospheric radiation, *Sci. Rep. WR 2003-01*, Koninklijk Ned. Meteorol. Inst., De Bilt, Netherlands.

Torres, O., P. K. Bhartia, J. R. Herman, Z. Ahmad, and J. Gleason (1998), Derivation of aerosol properties from satellite measurements of backscattered ultraviolet radiation: Theoretical basis, *J. Geophys. Res.*, *103*(D14), 17,099–17,110.

Valks, P. J. M., A. J. M. Piters, J. C. Lambert, C. Zehner, and H. Kelder (2003), A fast delivery system for the retrieval of near real-time ozone columns from GOME data, *Int. J. Remote Sens.*, *24*, 423–436.

van de Hulst, H. C. (1981), *Light Scattering by Small Particles*, Dover, Mineola, N. Y.

van der A, R. J., H. J. Eskes, J. H. G. M. van Geffen, R. F. van Oss, A. J. M. Piters, P. J. M. Valks, and C. Zehner (2000), GOME Fast delivery and value-Added Products (GOFAP), *Eur. Space Agency Spec. Publ., SP-461*.

van der A, R. J., R. F. van Oss, A. J. M. Piters, J. P. F. Fortuin, Y. J. Meijer, and H. M. Kelder (2002), Ozone profile retrieval from recalibrated Global Ozone Monitoring Experiment data, *J. Geophys. Res.*, *107*(D15), 4239, doi:10.1029/2001JD000696.

van Soest, G., L. G. Tilstra, and P. Stammes (2005), Large-scale validation of SCIAMACHY reflectance in the ultraviolet, *Atmos. Chem. Phys. Discuss.*, *5*, 1771–1796.

Wellemeyer, C. G., S. L. Taylor, G. Jaross, M. T. DeLand, C. J. Seftor, G. Labow, T. J. Swissler, and R. P. Cebula (1996), Final report on Nimbus-7 TOMS version 7 calibration, NASA Contract. Rep. 4717, NASA, Washington, D. C.

P. Stammes, L. G. Tilstra, and G. van Soest, Royal Netherlands Meteorological Institute (KNMI), P.O. Box 201, NL-3730 AE De Bilt, Netherlands. (stammes@knmi.nl; tilstra@knmi.nl; soestvg@knmi.nl)